TAR DNA-binding protein 43 (TDP-43) liquid–liquid phase separation is mediated by just a few aromatic residues

Received for publication, November 19, 2017, and in revised form, March 5, 2018 Published, Papers in Press, March 6, 2018, DOI 10.1074/jbc.AC117.001037

Hao-Ru Li[‡], Wan-Chin Chiang[‡], Po-Chun Chou[‡], Won-Jing Wang[‡], and Jie-rong Huang[‡§1]

From the [‡]Institute of Biochemistry and Molecular Biology and the [§]Institute of Biomedical Informatics, National Yang-Ming University, No. 155 Section 2, Li-nong Street, Taipei 11221, Taiwan

Edited by Wolfgang Peti

Eukaryotic cells contain distinct organelles, but not all of these compartments are enclosed by membranes. Some intrinsically disordered proteins mediate membraneless organelle formation through liquid–liquid phase separation (LLPS). LLPS facilitates many biological functions such as regulating RNA stability and ribonucleoprotein assembly, and disruption of LLPS pathways has been implicated in several diseases. Proteins exhibiting LLPS typically have low sequence complexity and specific repeat motifs. These motifs promote multivalent connections with other molecules and the formation of higher-order oligomers, and their removal usually prevents LLPS. The intrinsically disordered C-terminal domain of TAR DNA-binding protein 43 (TDP-43), a protein involved in motor neuron disease and dementia lacks a dominant LLPS motif, however, and how this domain forms condensates is unclear. Using extensive mutagenesis of TDP-43, we demonstrate here that three tryptophan residues and, to a lesser extent, four other aromatic residues are most important for TDP-43 to undergo LLPS. Our results also suggested that only a few residues may be required for TDP-43 LLPS because the α-helical segment (spanning ~20 residues) in the middle part of the C-terminal domain tends to self-assemble, reducing the number of motifs required for forming a multivalent connection. Our results indicating that a self-associating α-helical element with a few key residues regulates condensate formation highlight a different type of LLPS involving intrinsically disordered regions. The C-terminal domain of TDP-43 contains ~50 disease-related mutations, with no clear physicochemical link between them. We propose that they may disrupt LLPS indirectly by interfering with the key residues identified here.

Eukaryotic cells have different membrane-enclosed compartments (1) but not all of these are enclosed by a lipid membrane. Membraneless organelles, such as the stress granules that regulate RNA stability or the nucleoli that regulate ribonucleoprotein assembly (2), are also biologically important. Both *in vitro* and in-cell experiments have shown that some of the proteins in membraneless organelles can reversibly form condensates through liquid–liquid phase separation (LLPS)[2] (reviewed in Refs. 3–7). Multivalency (the presence of multiple binding sites) is critical for LLPS, as highlighted by the importance of tandem-repeat Src homology 3 domains and polyproline-rich motifs for signal transduction in actin regulation (8). Intrinsically disordered proteins (IDPs) with low sequence complexity, repeated sequence motifs, and structural plasticity facilitate multivalent interactions, as has been shown for several RNA-binding proteins, including hnRNPs (9–12), FUS (11, 13–16), and Whi3 (17). These RNA-binding proteins maintain protein homeostasis in cells by storing RNA inside membraneless organelles, whereas it has also been suggested that their impaired or irreversible aggregation may lead to proteinaceous diseases (9, 13). Signal transduction and RNA storage are not the only functions of the condensates: the protein BuGz facilitates the assembly of microtubules (18); SPD-5 is a key scaffold protein in the nucleation of microtubules in pericentriolar material (19); gene silencing has been shown to involve the LLPS of heterochromatin proteins (20, 21); the protein Tau, implicated in Alzheimer's disease, has been shown to form condensates (22); and the yeast prion protein Sub35 undergoes LLPS in response to cellular stress (23). Our previous study also suggests that the LLPS of galectin-3's low-complexity N-terminal domain is important for the formation of extracellular galectin-glycan lattices (24).

A number of amino acid motifs in IDPs with low sequence complexity are known to facilitate LLPS: for instance, tyrosines flanked with glycine or serine in FUS protein (11), the large number of FG and RG dipeptide repeats in Ddx4 (25), arginine-rich dipeptide repeats in C9orf72 (26), or the prevalence of negatively charged and aromatic/hydrophobic residues in the disordered domain of nephrin (27); and nucleoporins multivalently interact with transport factors through their FG repeats, hinting at a similar tendency to form condensates (28, 29). In these proteins, the formation of multivalent connections is facilitated by the presence of dozens of these motifs. In contrast, there is no dominant LLPS motif in the intrinsically disordered C-terminal domain of the TAR DNA-binding protein of 43 kDa (TDP-43; Fig. 1), which also forms condensates (9, 30–32): this ~160-residue domain contains only six positively and three negatively charged amino acids, four typical (G/S)-

This work was supported by the Ministry of Science and Technology of Taiwan Grants 106-2113-M-010-005-MY2 (to J. R. H.), 106-2633-B-009-001, and 105-2628-B-010-004-MY3 (to W. J. W.). The authors declare that they have no conflicts of interest with the contents of this article.
This article contains Movie S1, Figs. S1–S6, and Table S1.

[1] To whom correspondence should be addressed. Tel.: 886-2-2826-7258; E-mail: jierongh@ym.edu.tw.

[2] The abbreviations used are: LLPS, liquid–liquid phase separation; IDP, intrinsically disordered protein; hnRNP, heterogeneous nuclear ribonucleoprotein; TDP-43, TAR DNA-binding protein of 43 kDa; ALS, amyotrophic lateral sclerosis; HSQC, heteronuclear single-quantum coherence.

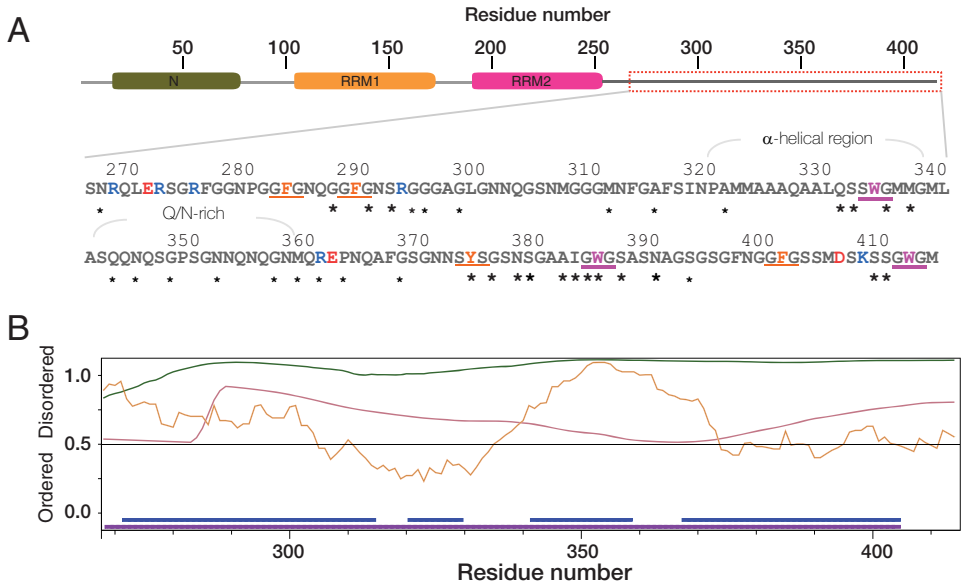

Figure 1. Amino acid sequence of the C-terminal domain of TDP-43 and the prediction of structural disorder and sequence complexity. *A,* the (G/S)-(F/Y)-(G/S) motif is colored in *orange* and the three tryptophans are colored *purple*. Positive and negatively charged residues are shown in *blue* and *red,* respectively. The locations of known ALS-associated mutations are indicated with *stars*. Those close to the motifs are shown in *enlarged font*. *B,* disorder predictions using the PONDR VSL2 (*green*) and VL3 (*red*) (62, 63), and the IUPRED (*orange*) (64) algorithms based on the primary sequence. Sequence complexity was calculated using the SEG algorithm (65) and the two main regions predicted with low sequence complexity are indicated with *blue* and *purple bars*, respectively.

(F/Y)-(G/S) LLPS motifs, and three sparsely distributed FG repeats (Fig. 1*A*). How this intrinsically disordered domain forms condensates using relatively few LLPS motifs is an open question. One of the main differences between TDP-43 and other IDP LLPS systems is its central α-helical element (residues ~320–340) (30, 31, 33), which is critical for forming condensates (30, 32). This α-helix assists intermolecular self-association (30, 31), and we have shown in a previous study (31) that LLPS is driven by hydrophobicity and inhibited by electrostatic repulsion. Although we demonstrated that removing a hydrophobic tryptophan in this α-helix severely disrupts LLPS (31), we did not untangle the network through which TDP-43 molecules make multivalent contacts using these sparse LLPS motifs. Here, we use mutagenesis to systematically investigate the effects on LLPS of seven aromatic residues that precede or follow glycine or serine (Fig. 1). We show that the most important elements for TDP-43 LLPS are the three tryptophans in this domain, especially Trp-334, whereas other aromatic motifs contribute to a lesser extent. This mechanism, involving just a few repeated motifs and an α-helical assembly center, is different from those previously described for LLPS and provides a new perspective on the disease-associated mutations of TDP-43.

Results

TDP-43 liquid–liquid phase separation

In addition to its functions in gene regulation and mRNA transportation (34), TDP-43 has been identified as the main disease protein in the biopsies of amyotrophic lateral sclerosis (ALS) patients (35). Like many other ALS-associated RNA-binding proteins such as FUS, some hnRNPs, and TIA-1 (36), TDP-43 has been shown to undergo LLPS (9). It has been suggested, furthermore, that the disruption of LLPS increases the pathological fibrilization of these proteins (36). The mechanism governing LLPS for TDP-43 is therefore important for its pathogenicity. Cell-based studies have demonstrated that TDP-43 droplet-like properties are inducible under certain conditions (32, 37). Conicella *et al.* (30) have also characterized in detail the LLPS properties of the C-terminal domain of TDP-43 *in vitro*. They reported that this domain only undergoes LLPS in the presence of ions or RNA molecules (30), whereas with a slightly different construct and buffer conditions, we induced LLPS of TDP-43 at low temperatures in the absence of salt or RNA molecules (31). We measured the turbidity of the WT sample (the optical density at 600 nm, $OD_{600\,nm}$, Fig. 2*A*) and recorded micrographs of the condensates at different static temperatures (Fig. 2*B*) to confirm the occurrence of LLPS. We also collected time-lapse micrographs from low to high and then back to low temperatures to confirm the reversibility of the process (Fig. 2*C*, and supporting Movie S1). Although turbidity depends on both the number and the size of the particles, the TDP-43 condensates were all found to be around 1 μm in diameter (Fig. 2*B* and supporting Fig. S1) in agreement with Molliex *et al.*'s observation (9). This situation differs from the spread of condensate sizes usually observed for LLPS proteins. For TDP-43 therefore, turbidity reflects only the number of particles present. We thus used the turbidity of the sample, supported by micrographs, to indicate the presence of LLPS. We measured the turbidity and collected microscopic images of the ALS-related mutants Q331K (net charge increased from +3 to +4) and A315E (net charge reduced from +3 to +2), artificial W334G (removal of a hydrophobic residue), the Q331K variant in the presence of NaCl (screening of charge-charge interactions), and the WT in the presence of urea or 1,6-hexanediol (disruption of hydrophobic interactions) to confirm that LLPS occurs as a competition between

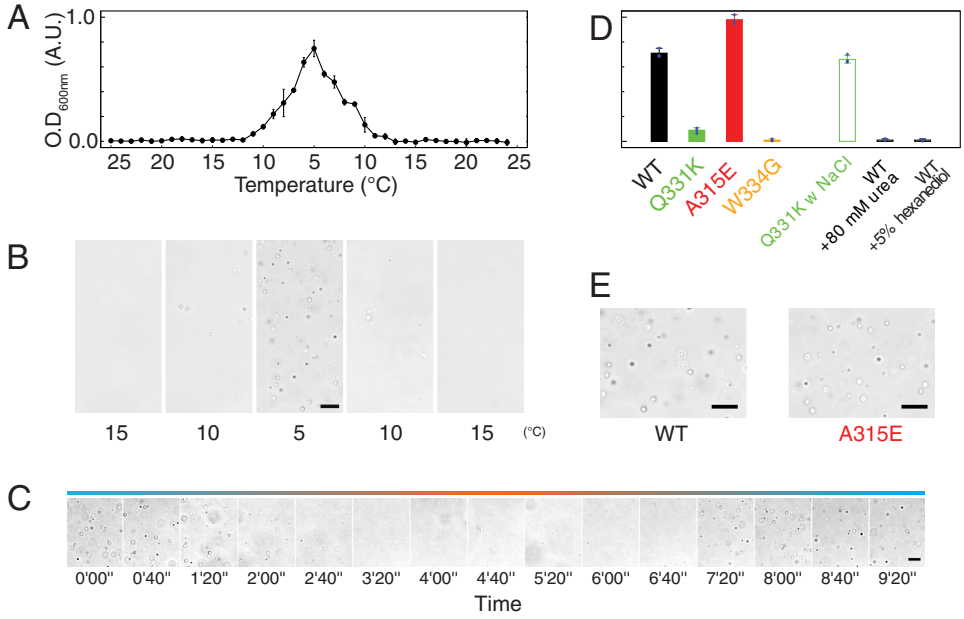

Figure 2. Liquid–liquid phase separation of the C-terminal domain of TDP-43. *A,* the optical density at 600 nm ($OD_{600\ nm}$) of a 20 μM WT sample at different temperatures, highlighting the reversibility of the process. *B,* micrographs (*scale bar*: 10 μm) at different static temperatures. *C,* time-lapse micrographs demonstrating the reversibility of condensate formation (see "Experimental procedures" for details of how these images were collected). *D,* turbidity measured at 5 °C for different mutants in a 10 mM phosphate buffer at pH 6.5 only (*solid bars*) or with additional compounds (NaCl, urea, or hexanediol, *open bars*). *E,* micrographs from the samples whose turbidity is shown in *panel D*.

hydrophobic and electrostatic forces, as we demonstrated previously using different buffer conditions (Fig. 2, *D* and *E*) (31). NMR spectroscopy analysis shows that these mutations and different buffer conditions have little effect on the α-helical propensity of the central domain (Ref. 31 and supporting Fig. S2).

The three key tryptophans critical for LLPS

In our previous study, we demonstrated that replacing hydrophobic Trp-334 with glycine disrupts LLPS despite favorable conditions, *i.e.* high protein concentration (40 μM), high NaCl concentration (300 mM), and low temperature (5 °C) (31). We also noted that LLPS still occurs for W334G when the protein concentration is greater than 100 μM. (Note that all the ALS-associated mutants we have studied and the WT precipitate rapidly when the protein concentration is higher than 40 μM under our standard buffer conditions: pH 6.5, 10 mM phosphate buffer.) Increasing the protein concentration increases the chance for the protein molecules to interact with one another and thus compensates for the loss of the attraction from Trp-334 driven by the hydrophobic interaction. A single residue, however, is unlikely to disrupt all the multivalent contacts that contribute to forming the higher-order assembly unless this assembly is divalent. Trp-334 follows a serine and precedes a glycine residue, which is reminiscent of a recognized LLPS motif: tyrosine or phenylalanine flanked by glycine or serine (10, 11, 14). It is noteworthy that there are only three tryptophans in the C-terminal domain, and all three present this motif (Trp-334, Trp-385, and Trp-412, *purple bars* in Fig. 1). Conicella *et al.* (30) performed intermolecular paramagnetic relaxation enhancement studies using a nitroxide spin-label introduced at residue 317 and observed enhanced NMR relaxation rates from the central α-helix of one molecule to that of another and between the middle α-helix and residues 382–385 (containing Trp-385). Although this was not mentioned in the original study, the relaxation rates of residues ~400–412 were also increased, indicating contacts between the spin label at position 317 and the region around Trp-412. Furthermore, tryptophans have been shown to initiate the refolding of a denatured protein in acidic urea (38), which also suggests that tryptophans may initiate higher-order intermolecular assembly.

In light of these studies, our hypothesis was that the three tryptophans are involved in the initiation of LLPS and may form multivalent connections by themselves. To understand the importance of each tryptophan for LLPS, we created all possible tryptophan-to-glycine constructs and used the turbidity and micrographs of the corresponding samples under conditions favoring condensate formation. At 5 °C and a protein concentration of 20 μM, clear evidence of LLPS was only observed for the WT sample (Fig. 3*A*). In the presence of 100 mM NaCl at the same protein concentration (Fig. 3, *B* and *D*, and supporting Fig. S1), the only constructs for which increased turbidity and condensates in the micrographs were observed were two single tryptophan-replaced (Δ1W) variants: W385G and W412G. When we increased the protein concentration to 100 μM but without salt, all three Δ1W variants showed signs of LLPS with W385G and W412G having a stronger phase separation tendency than W334G (Fig. 3, *C* and *D,* and supporting Fig. S1). Under these conditions, condensates and increased turbidity were observed for all three double-tryptophan (Δ2W) mutants, more so for the W385G/W412G variant than the W334G/W385G and W334G/W412G variants. There were almost no detectable signs of LLPS for the triple-tryptophan (Δ3W) mutant, W334G/W385G/W412G. When salt was added at this high protein concentration, the W385G and W412G samples

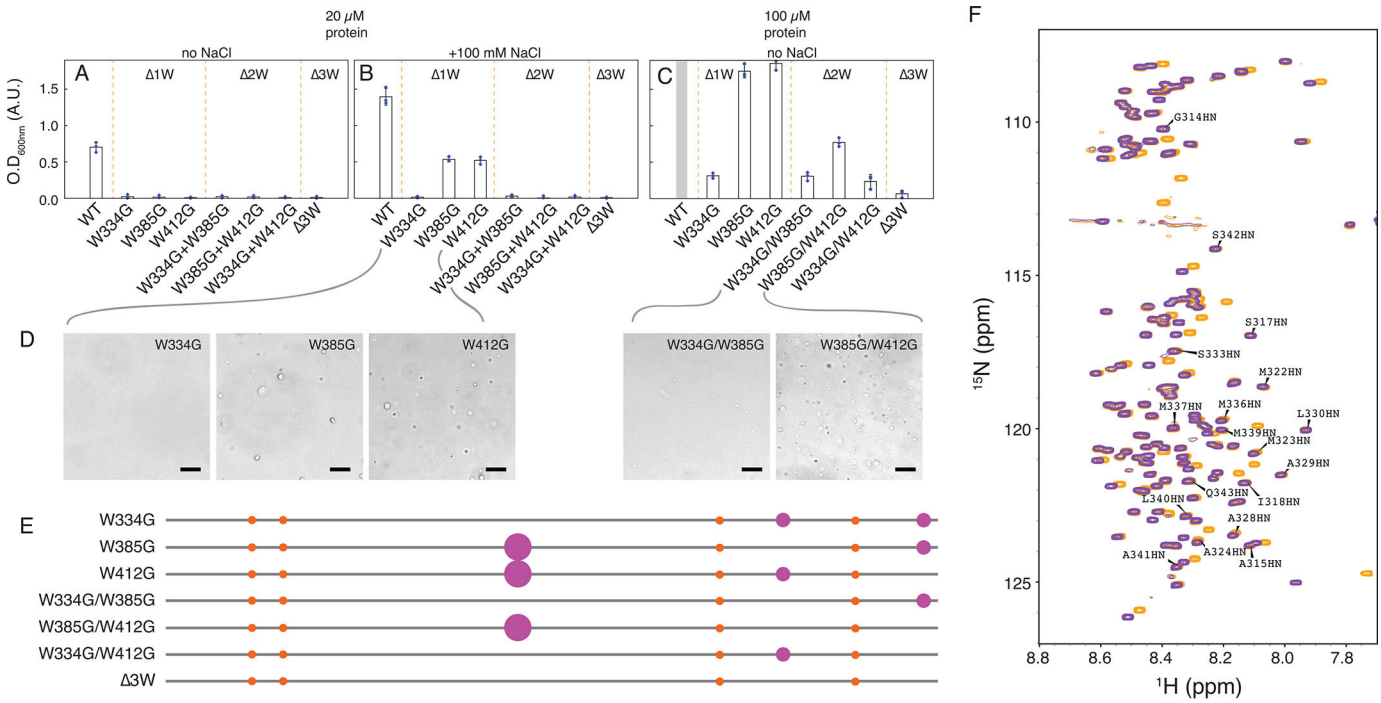

Figure 3. Turbidity of samples of WT TDP-43 and tryptophan-to-glycine variants. All data were collected at 5 °C. *A* and *B*, turbidity of 20 μM protein samples (*A*) in the absence and (*B*) in the presence of 100 mM NaCl. *C*, turbidity of 100 μM protein samples in the absence of 100 mM NaCl. The *gray bars* indicate samples that precipitated before measurements could be taken, the *error bars* represent the standard deviation of three repeated measurements (*blue squares*). *D*, micrographs of the variants for which there is clear evidence of condensation in *panels B* and *C* (*scale bar*, 10 μm). *E*, schematic representations of the constructs. *F*, comparison of HSQC spectra between W334G and Δ3W. The HSQC spectrum of the W334G variant (*orange*) is overlaid on the Δ3W mutant (*purple*). Most of the cross-peaks overlap apart from those close to the mutation sites. The cross-peaks from residues in the α-helical region are highlighted.

precipitated immediately (Fig. S3) and the Δ2W variants followed a similar trend to the one shown in Fig. 3*C*, namely that the strongest signs of LLPS were observed for the variant with Trp-334 retained (W385G/W412G). The turbidity of the Δ3W sample was insignificant. We also performed the experiments "reversibly," to demonstrate that the samples with zero optical density do still contain protein molecules. We centrifuged 100 μM samples at 15,000 × *g* at 5 °C for 5 min with a higher protein concentration in the supernatant indicating a lesser propensity for LLPS. The results are consistent (Fig. S4).

These results indicate that Trp-334 is the most important of the three tryptophans for LLPS, as its removal severely reduces the LLPS tendency of the corresponding WT and disease related variants under the conditions considered here (Figs. 2*D* and 3*B*). Only when the protein concentration is increased to 100 μM are condensates observed for the W334G variant. The 20 μM samples of the W385G and W412G mutants are more prone to LLPS than W334G (Fig. 3, *B–D*), reinforcing this interpretation that Trp-334 is more important than Trp-385 or Trp-412 for LLPS. The Δ2W variants with Trp-334 removed (W334G/W385G and W334G/W412G) show much less of a tendency toward LLPS than the W385G/W412G variant, also in agreement with this interpretation. Although we do not have NMR chemical shift assignments for all these tryptophan mutants, we have shown previously that the W334G mutation, which is within the α-helical region, has little effect on its α-helical propensity (31). The good overlap between the NMR spectra of the W334G and Δ3W variants (Fig. 3*F*), especially for cross-peaks from residues in the α-helix, indicates that their conformations are similar.

The LLPS network between tryptophans and other motif residues

Because alanine is generally regarded as being as hydrophobic as tryptophan (39) or more so (40, 41), and has a greater α-helical propensity (42), we replaced Trp-334 with alanine to investigate the role of hydrophobicity and secondary structure in TDP-43's LLPS. (Note that we did not insert phenylalanine or tyrosine because (G/S)-(F/Y)-(G/S) is also an LLPS motif.) Samples of the W334A (unaltered or increased hydrophobicity) variant were found to have a similar turbidity to those of the W334G (reduced hydrophobicity) variant under all conditions, suggesting that Trp-334 is involved in intermolecular multivalent linking (Fig. 4).

The Δ2W construct with Trp-334 retained (W385G/W412G) still shows signs of LLPS when the protein concentration is high (100 μM, Fig. 3, *C* and *D*), indicating that residues other than the three tryptophans are involved in the formation of condensates (*i.e.* it is not simply a trivalent network that drives LLPS). Accordingly, we introduced glycines to replace the single tyrosine and three phenylalanine residues in (G/S)-(F/Y)-(G/S) motifs in the W385G/W412G variant, leaving Trp-334 only in place (*i.e.* Δ2W.Δ3F.Δ1Y in the nomenclature introduced above). No increase in turbidity was observed for this construct under any conditions, nor were any condensates observed in the micrographs (Fig. 4), as was the case for the Δ3W variant. These results for the Δ2W (W385G/W412G) and Δ2W.Δ3F.Δ1Y constructs indicate that the corresponding tyrosine and phenylalanine residues are also involved in the formation of condensates. However, their contribution is

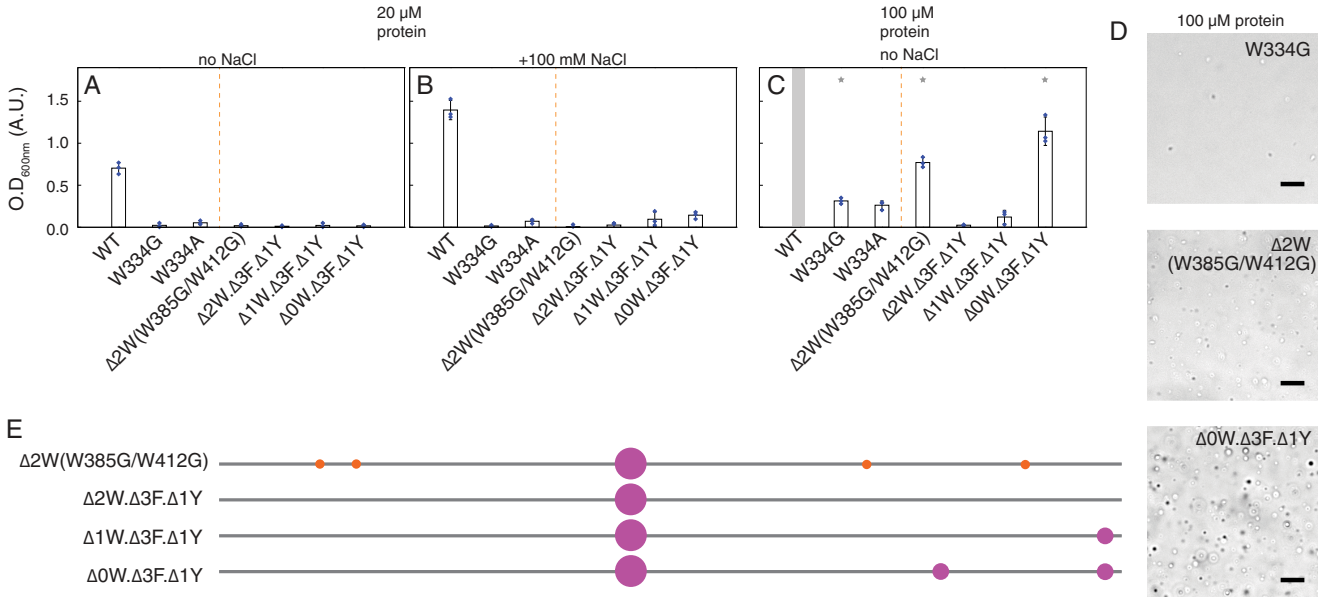

Figure 4. Turbidity of samples of WT TDP-43 and W334A and other phenylalanine-to-glycine and tyrosine-to-glycine variants. All data were collected at 5 °C. *A* and *B,* turbidity of 20 μM protein samples (*A*) in the absence and (*B*) in the presence of 100 mM NaCl. *C*, turbidity of 100 μM protein samples in the absence of 100 mM NaCl. The *gray bars* indicate samples that precipitated before measurements could be taken, the *error bars* represent the standard deviation of three repeated measurements (*blue squares*). *D,* comparison of micrographs of some of the variants indicated with *gray stars* in *panel C* (*scale bar*, 10 μm). *E,* schematic representations of the constructs.

weaker than that of the tryptophans. Indeed, condensates were observed once more when one or both of the mutated tryptophans were reintroduced (respectively Δ1W.Δ3F.Δ1Y and Δ0W.Δ3F.Δ1Y, Fig. 4, *C* and *D*).

Supporting Fig. S2 shows that mutating Trp-334 has no effect on the structural propensity of the α-helical region. Because all the other mutations investigated here affect residues outside the α-helical region, one can assume that the α-helical propensity is likewise unchanged in these variants. This would also be consistent with our studies of ALS-associated mutants: G298S, Q331K, M337V (31), A315E in this study (Fig. S2), G294V, G294A, and A315T variants (Fig. S5), and data from other groups (30, 33).

NMR spectroscopy indicates that self-association is enhanced in the presence of Trp-334

In our previous work, we showed using NMR peak intensity ratios and chemical shift perturbations between 40 and 20 μM samples and that the α-helical region (residues 320–340) of the C-terminal domain TDP-43 self-associates. The NMR peak intensity ratio in the α-helical region is less than would be expected from the change in protein concentration, indicating a shift in equilibrium from the monomeric to the self-associated state, as shown also by the chemical shift differences (31). These two NMR parameters are more difficult to measure for the mutants studied here because they are less prone to undergo LLPS so we increased the concentration ratios from two to five (*i.e.* we compared 100 and 20 μM samples). We collected NMR spectra at 15 °C, a temperature at which no condensate is observed but self-association still occurs (31). For W334G, self-association of the α-helix between protein molecules still occurs: the signal ratios for the α-helical region are slightly less than the expected five-to-one ratio and there are small changes in chemical shift between the two concentrations (*upper panels* in Fig. 5, *A* and *B*, and supporting Fig. S6*A*). Replacing Trp-334 with hydrophobic alanine does not recover self-association (*middle panels* in Fig. 5, *A* and *B*, and supporting Fig. S6*B*). These results for the W334G and W334A variants imply that the self-association tendency of the α-helical element is independent from the effects of Trp-334. On the other hand, removing all the aromatic residues in LLPS motifs except Trp-334 (Δ2W.Δ3F.Δ1Y), leads to more self-association than in the variants without Trp-334 (*bottom panels* in Fig. 5, *A–C*). This indicates that Trp-334 strongly enhances the self-association of the α-helix. However, the Δ2W.Δ3F.Δ1Y variant does not form condensates (Fig. 4*C*) because even though it self-associates more, multivalent contacts are still required for the protein to undergo LLPS.

Discussion

Protein multivalency is crucial for the assembly of higher-order oligomers (8). Intrinsically disordered regions favor higher-order assembly, but those with a low sequence complexity are more likely to be multivalent (11). These simple sequences often contain repeated patterns that act as alternative contact sites. For example, clustered blocks of positively and negatively charged residues are critical for the LLPS of Ddx4 (25), and (G/S)-(F/Y)-(G/S) motifs have been identified as important for LLPS in FUS protein (11). On the other hand, in the case of complex coacervation for the C-terminal domain of nephrin, the total charge composition is more important than the primary sequence (27), suggesting that hybrid connections between charged and aromatic/hydrophobic residues are involved. Systematically removing these patterns or motifs gradually reduces the LLPS tendency of the corresponding constructs, as shown in a recent study in which any consecutive 5 of the 27 tyrosines in an IDP were show to be of equal importance for phase separation (16). Of the 25 tyrosine or phenylalanine residues in hnRNP A2 on the other hand,

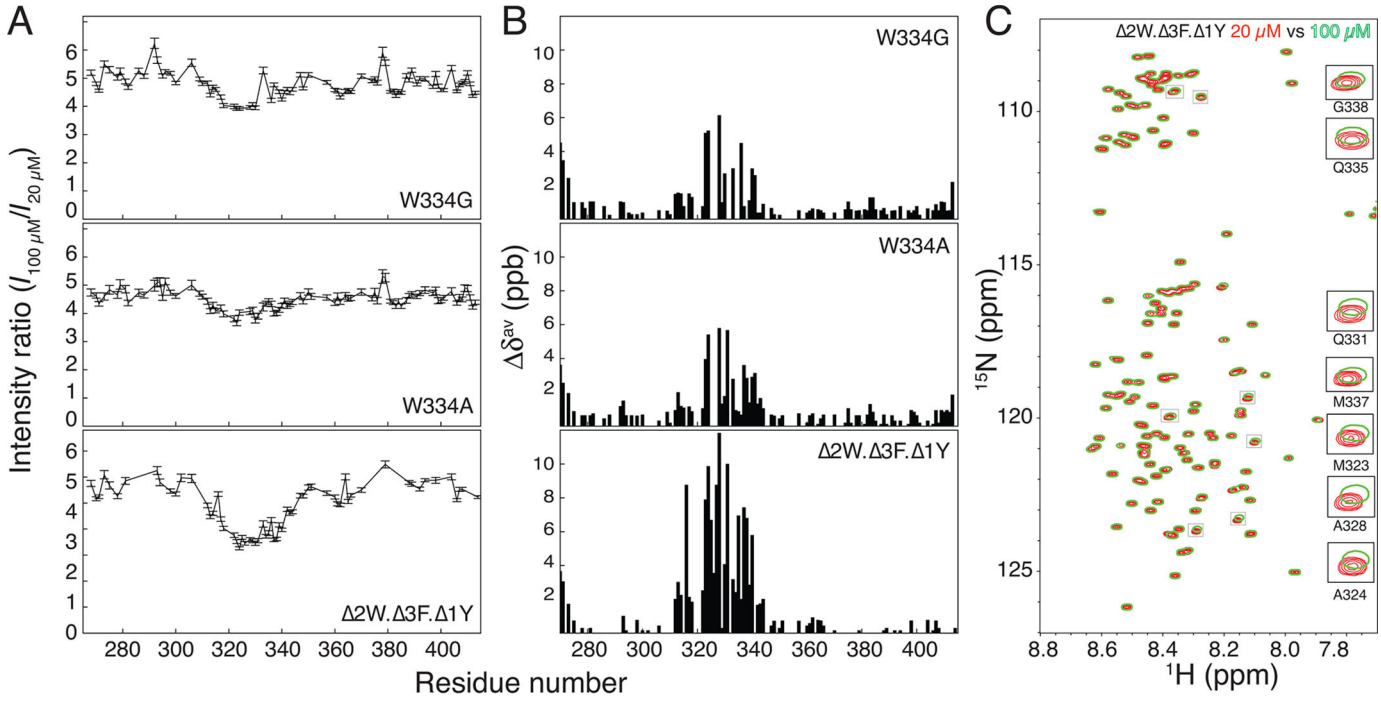

Figure 5. NMR signal intensity ratios and chemical shift perturbations between 100 and 20 μM protein samples. *A,* signal intensity ratios and *B,* chemical shift perturbations between 100 and 20 μM samples of W334G, W334A, and Δ2W.Δ3F.Δ1Y variants of TDP-43. *C,* HSQC spectra of the 20 μM (*red*) and 100 μM (*green*) samples of the Δ2W.Δ3F.Δ1Y variant. The most pronounced changes in chemical shift are highlighted.

about 11, clustered in a specific block, have been shown to be more important than the others for LLPS (12). The mechanism of LLPS for the C-terminal domain of TDP-43 is different, however, because only a small number of residues are involved. The most important of these is Trp-334, followed by Trp-385 and Trp-412. When the latter two tryptophans are removed, LLPS still occurs at 5 °C but only at high protein and high salt concentrations, whereas it does not when all the aromatic residues in LLPS motifs other than Trp-334 are removed, suggesting that these aromatic residues are involved in LLPS but to a lesser extent.

Why is LLPS controlled by just a few residues in TDP-43?

Multivalent connections in IDPs that undergo LLPS typically involve a large number of different motifs (11, 25) or specific types of residues (27) distributed throughout the amino acid sequence. For the C-terminal domain of TDP-43, however, LLPS is driven by just three tryptophans with minor contributions from one tyrosine and three phenylalanines. One potential reason why LLPS is controlled by fewer motifs in the C-terminal domain of TDP-43 is the presence of an α-helix. This element spans roughly 20 residues in the center of the domain (Fig. 1) and is involved in intermolecular interactions (30, 31). It is highly conserved (32) and mediates pre-mRNA splicing through interactions with other hnRNP proteins (43–45). Deleting this α-helical region or reducing its secondary structure propensity by point mutations or by inserting random sequences (30, 32) prevents LLPS. Moreover, as demonstrated in model polyalanine and polyglutamine systems, Polling *et al.* (46) suggest that polyalanine-formed α-helices can promote self-assembly. They also suggest that α-helical driven clustering may facilitate the nucleation of amyloid fibrils when, as for polyadenylate-binding nuclear protein 1, the fibril-promoting region is outside the polyalanine stretch. The C-terminal domain of TDP-43 has a similar sequence arrangement: the QN-rich domain that follows the α-helix (Fig. 1) is known to be involved in the protein's aggregation (47–49). Trp-334 in this α-helix may enhance the intrinsic tendency toward self-assembly of the helical element (Fig. 5), and this enhanced intermolecular interaction may thus facilitate LLPS. There is less self-association in the absence of the α-helix so many more LLPS motifs would be required to sufficiently increase the chance of intermolecular contacts via weak electrostatic interactions, hydrophobicity, and/or translational diffusion. A large number of repeated LLPS motifs may be an evolutionary advantage (25, 50). However, by bringing the molecules closer together, the α-helix reduces the number of motifs required to form higher-order assemblies.

It has been shown for several proteins that a reduced tendency toward LLPS increases the likelihood of pathological aggregation (9, 13). There are around 50 ALS-associated variants of the C-terminal domain of TDP-43 but no clear physiochemical link between the corresponding mutations. It has recently been reported that the phosphorylation of FUS protein close to LLPS-related tyrosine sites may cause disease (15, 16). Several of the ALS-associated mutations of TDP-43 (*black stars* in Fig. 1*A*) and the Ser-409 and Ser-410 phosphorylation sites (51, 52) are also close to the LLPS motifs we identified here. Studying the effect of these ALS mutants on LLPS motifs may offer an alternative avenue toward understanding the cause of this disease and others. Furthermore, the fact that the LLPS of this intrinsically disordered domain is controlled by just a few residues may explain the unusual droplet form of TDP-43 (9).

Table 1
Extinction coefficients and 1% absorbance used to determine protein concentrations
The extinction coefficient is at 280 nm measured in water. The values were determined based on the primary sequence using the ProtParam function (web.expasy.org/protparam/) on the ExPASy server.

Constructs	Extinction coefficient	$A_{280\ nm}$ (1%, g/100 ml)
WT	17,990	11.31
W334G	12,490	7.92
W334A	12,490	7.91
W385G	12,490	7.92
W412G	12,490	7.92
W334G/W385G	6,990	4.47
W385G/W412G	6,990	4.47
W412G/W334G	6,990	4.47
Δ3W	1,490	0.96
Δ2W.Δ3F.Δ1Y	5,500	3.6
Δ1W.Δ3F.Δ1Y	11,000	7.14
Δ0W.Δ3F.Δ1Y	16,500	10.62

Experimental procedures

Protein expression and purification

The constructs of the C-terminal domain of TDP-43 (residues 266–414) were prepared using a His_6 tag as described previously (31, 53). This purification tag has no effect on the α-helical propensity or the LLPS tendency of the domain (31). Most mutants were created using a designed primer (Table S1). The Δ2W.Δ3F.Δ1Y construct was created by whole gene synthesis and the Δ1W.Δ3F.Δ1Y and Δ0W.Δ3F.Δ1Y constructs were created with adapted primers (Table S1). All constructs were verified by DNA sequencing. The same protein expression, purification, and sample quality control protocols were used as described in our previous publication (31). In short, the overexpressed protein was extracted from inclusion bodies using 8 M urea and purified using a nickel-charged immobilized metal-ion affinity chromatography column (Qiagen, Inc.) and then a C4 reverse phase column (Thermo Scientific, Inc.) using an HPLC system. The purified sample was lyophilized for storage, and then dissolved in 10 mM phosphate buffer at pH 6.5 for experiments. The protein concentration was determined using the Beer-Lambert law by measuring the absorbance at 280 nm using a NanoDrop UV-visible spectrometer (Thermo Scientific, Inc.) with the appropriate extinction coefficients (Table 1). The extinction coefficients were calculated based on the primary sequence using the web server ExPASy (54).

Turbidity measurements

The turbidity of the protein samples was quantified by measuring light transmittance at 600 nm using a JASCO V550 UV-visible spectrophotometer. The temperature of the spectrophotometer was controlled using a water bath. For each measurement, the sample was left to equilibrate in the temperature-controlled water bath for 5 min. Ten scans were accumulated for each measurement and measurements at each temperature point were repeated three times to estimate the associated errors. The data are reported as mean ± S.D. The samples were all left to return to room temperature after each measurement to confirm the reversibility of the LLPS process.

Microscopy

The micrographs were collected using an Olympus BX51 microscope with a ×40 long working distance objective lens. The images were recorded with a Zeiss AxioCam MRm camera. The protein samples were placed on a thermostatic microscope stage (THMS600, Linkam Scientific Inc.) and were equilibrated for 5 min at each temperature before recording the micrographs.

For the time-lapse micrographs, the samples were put into the sample chamber pre-equilibrated at 0 °C. Once the number of condensates ceased to increase, the temperature of the chamber was changed to 25 °C and the first micrograph was recorded (time zero). When all the condensates had disappeared, the temperature was immediately changed to 0 °C. Micrographs were collected every 10 s (Fig. 2*C* shows two images recorded 40 s apart, and supporting Movie S1 shows the time-lapse movie).

NMR spectroscopy

^{15}N-edited heteronuclear single-quantum coherence (HSQC) spectra were recorded using the standard pulse sequence and the WATERGATE scheme to suppress solvent signal (55, 56). To confirm the quality and integrity of the samples, one-dimensional proton spectra were recorded with an improved WATERGATE solvent saturation scheme (57) before and after all NMR experiments. Standard chemical shift assignment experiments were recorded with nonuniform sampling schemes (58, 59). All spectra were recorded on a Bruker AVIII 600 MHz spectrometer with a cryogenic probe. The data were processed using NMRPipe (60). Kjaergaard *et al.*'s (61) database of random-coil shifts was used for secondary chemical shift analysis. The procedure used to analyze the peak intensities has been described in detail previously (31). Briefly, the nonlinear line shape modeling function in NMRPipe was applied to all the HSQC spectra, with a Lorenzian-to-Gaussian window function. The averaged chemical shift difference ($\Delta\delta^{av}$) was calculated using,

$$\Delta\delta^{av} = \sqrt{\frac{(\Delta\delta_H)^2 + \left(\frac{1}{5}\Delta\delta_N\right)^2}{2}} \quad \text{(Eq. 1)}$$

where $\Delta\delta_H$ and $\Delta\delta_N$ are the chemical shift differences between two ^{1}H-^{15}N HSQC spectra, respectively, for the amide proton and the nitrogen chemical shifts.

Concentration measurements after centrifugation

Different 100 μM protein samples were prepared in 1.5-ml Eppendorf tubes. The samples were centrifuged at 15,000 × *g* at 5 °C for 5 min. The concentration of the supernatants was measured using a NanoDrop spectrometer. The experiments were repeated three times for each variant. The results are reported as mean ± S.D.

Author contributions—H.-R. L. and J.-r. H. conceptualization; H.-R. L. and W.-C. C. data curation; H.-R. L., W.-C. C., P.-C. C., and J.-r. H. formal analysis; H.-R. L., P.-C. C., and J.-r. H. investigation; H.-R. L., W.-J. W., and J.-r. H. methodology; P.-C. C. visualization; W.-J. W. and J.-r. H. resources; W.-J. W. and J.-r. H. supervision; W.-J. W. and J.-r. H. funding acquisition; J.-r. H. writing-original draft; J.-r. H. project administration; J.-r. H. writing-review and editing.

Acknowledgment—We thank Professor Mei-Lin Ho (Soochow University) for access to the temperature-controlled microscope stage.

References

1. Warren, G., and Wickner, W. (1996) Organelle inheritance. *Cell* **84,** 395–400 CrossRef Medline
2. Courchaine, E. M., Lu, A., and Neugebauer, K. M. (2016) Droplet organelles? *EMBO J.* **35,** 1603–1612 CrossRef Medline
3. Hyman, A. A., Weber, C. A., and Jülicher, F. (2014) Liquid-liquid phase separation in biology. *Annu. Rev. Cell Dev. Biol.* **30,** 39–58 CrossRef Medline
4. Guo, L., and Shorter, J. (2015) It's raining liquids: RNA tunes viscoelasticity and dynamics of membraneless organelles. *Mol. Cell* **60,** 189–192 CrossRef Medline
5. Chong, P. A., and Forman-Kay, J. D. (2016) Liquid-liquid phase separation in cellular signaling systems. *Curr. Opin. Struct. Biol.* **41,** 180–186 CrossRef Medline
6. Banani, S. F., Lee, H. O., Hyman, A. A., and Rosen, M. K. (2017) Biomolecular condensates: organizers of cellular biochemistry. *Nat. Rev. Mol. Cell Biol.* **18,** 285–298 CrossRef Medline
7. Shin, Y., and Brangwynne, C. P. (2017) Liquid phase condensation in cell physiology and disease. *Science* **357,** eaaf4382 CrossRef Medline
8. Li, P., Banjade, S., Cheng, H. C., Kim, S., Chen, B., Guo, L., Llaguno, M., Hollingsworth, J. V., King, D. S., Banani, S. F., Russo, P. S., Jiang, Q. X., Nixon, B. T., and Rosen, M. K. (2012) Phase transitions in the assembly of multivalent signalling proteins. *Nature* **483,** 336–340 CrossRef Medline
9. Molliex, A., Temirov, J., Lee, J., Coughlin, M., Kanagaraj, A. P., Kim, H. J., Mittag, T., and Taylor, J. P. (2015) Phase separation by low complexity domains promotes stress granule assembly and drives pathological fibrillization. *Cell* **163,** 123–133 CrossRef Medline
10. Lin, Y., Protter, D. S., Rosen, M. K., and Parker, R. (2015) Formation and maturation of phase-separated liquid droplets by RNA-binding proteins. *Mol. Cell* **60,** 208–219 CrossRef Medline
11. Kato, M., Han, T. W., Xie, S., Shi, K., Du, X., Wu, L. C., Mirzaei, H., Goldsmith, E. J., Longgood, J., Pei, J., Grishin, N. V., Frantz, D. E., Schneider, J. W., Chen, S., Li, L., *et al.* (2012) Cell-free formation of RNA granules: low complexity sequence domains form dynamic fibers within hydrogels. *Cell* **149,** 753–767 CrossRef Medline
12. Xiang, S., Kato, M., Wu, L. C., Lin, Y., Ding, M., Zhang, Y., Yu, Y., and McKnight, S. L. (2015) The LC domain of hnRNPA2 adopts similar conformations in hydrogel polymers, liquid-like droplets, and nuclei. *Cell* **163,** 829–839 CrossRef Medline
13. Patel, A., Lee, H. O., Jawerth, L., Maharana, S., Jahnel, M., Hein, M. Y., Stoynov, S., Mahamid, J., Saha, S., Franzmann, T. M., Pozniakovski, A., Poser, I., Maghelli, N., Royer, L. A., Weigert, M., *et al.* (2015) A liquid-to-solid phase transition of the ALS protein FUS accelerated by disease mutation. *Cell* **162,** 1066–1077 CrossRef Medline
14. Burke, K. A., Janke, A. M., Rhine, C. L., and Fawzi, N. L. (2015) Residue-by-residue view of *in vitro* FUS granules that bind the C-terminal domain of RNA polymerase II. *Mol. Cell* **60,** 231–241 CrossRef Medline
15. Monahan, Z., Ryan, V. H., Janke, A. M., Burke, K. A., Rhoads, S. N., Zerze, G. H., O'Meally, R., Dignon, G. L., Conicella, A. E., Zheng, W., Best, R. B., Cole, R. N., Mittal, J., Shewmaker, F., and Fawzi, N. L. (2017) Phosphorylation of the FUS low-complexity domain disrupts phase separation, aggregation, and toxicity. *EMBO J.* **36,** 2951–2967 CrossRef Medline
16. Lin, Y., Currie, S. L., and Rosen, M. K. (2017) Intrinsically disordered sequences enable modulation of protein phase separation through distributed tyrosine motifs. *J. Biol. Chem.* **292,** 19110–19120 CrossRef Medline
17. Zhang, H., Elbaum-Garfinkle, S., Langdon, E. M., Taylor, N., Occhipinti, P., Bridges, A. A., Brangwynne, C. P., and Gladfelter, A. S. (2015) RNA controls polyQ protein phase transitions. *Mol. Cell* **60,** 220–230 CrossRef Medline
18. Jiang, H., Wang, S., Huang, Y., He, X., Cui, H., Zhu, X., and Zheng, Y. (2015) Phase transition of spindle-associated protein regulate spindle apparatus assembly. *Cell* **163,** 108–122 CrossRef Medline
19. Woodruff, J. B., Ferreira Gomes, B., Widlund, P. O., Mahamid, J., Honigmann, A., and Hyman, A. A. (2017) The centrosome is a selective condensate that nucleates microtubules by concentrating tubulin. *Cell* **169,** 1066–1077.e1010 CrossRef Medline
20. Larson, A. G., Elnatan, D., Keenen, M. M., Trnka, M. J., Johnston, J. B., Burlingame, A. L., Agard, D. A., Redding, S., and Narlikar, G. J. (2017) Liquid droplet formation by HP1α suggests a role for phase separation in heterochromatin. *Nature* **547,** 236–240 CrossRef Medline
21. Strom, A. R., Emelyanov, A. V., Mir, M., Fyodorov, D. V., Darzacq, X., and Karpen, G. H. (2017) Phase separation drives heterochromatin domain formation. *Nature* **547,** 241–245 CrossRef Medline
22. Ambadipudi, S., Biernat, J., Riedel, D., Mandelkow, E., and Zweckstetter, M. (2017) Liquid-liquid phase separation of the microtubule-binding repeats of the Alzheimer-related protein Tau. *Nat. Commun.* **8,** 275 CrossRef Medline
23. Franzmann, T. M., Jahnel, M., Pozniakovsky, A., Mahamid, J., Holehouse, A. S., Nüske, E., Richter, D., Baumeister, W., Grill, S. W., Pappu, R. V., Hyman, A. A., and Alberti, S. (2018) Phase separation of a yeast prion protein promotes cellular fitness. *Science* **359,** eaao5654 CrossRef Medline
24. Lin, Y. H., Qiu, D. C., Chang, W. H., Yeh, Y. Q., Jeng, U. S., Liu, F. T., and Huang, J. R. (2017) The intrinsically disordered N-terminal domain of galectin-3 dynamically mediates multisite self-association of the protein through fuzzy interactions. *J. Biol. Chem.* **292,** 17845–17856 CrossRef Medline
25. Nott, T. J., Petsalaki, E., Farber, P., Jervis, D., Fussner, E., Plochowietz, A., Craggs, T. D., Bazett-Jones, D. P., Pawson, T., Forman-Kay, J. D., and Baldwin, A. J. (2015) Phase transition of a disordered nuage protein generates environmentally responsive membraneless organelles. *Mol. Cell* **57,** 936–947 CrossRef Medline
26. Boeynaems, S., Bogaert, E., Kovacs, D., Konijnenberg, A., Timmerman, E., Volkov, A., Guharoy, M., De Decker, M., Jaspers, T., Ryan, V. H., Janke, A. M., Baatsen, P., Vercruysse, T., Kolaitis, R. M., Daelemans, D., *et al.* (2017) Phase separation of C9orf72 dipeptide repeats perturbs stress granule dynamics. *Mol. Cell* **65,** 1044–1055.e1045 Medline
27. Pak, C. W., Kosno, M., Holehouse, A. S., Padrick, S. B., Mittal, A., Ali, R., Yunus, A. A., Liu, D. R., Pappu, R. V., and Rosen, M. K. (2016) Sequence determinants of intracellular phase separation by complex coacervation of a disordered protein. *Mol. Cell* **63,** 72–85 CrossRef Medline
28. Milles, S., Mercadante, D., Aramburu, I. V., Jensen, M. R., Banterle, N., Koehler, C., Tyagi, S., Clarke, J., Shammas, S. L., Blackledge, M., Gräter, F., and Lemke, E. A. (2015) Plasticity of an ultrafast interaction between nucleoporins and nuclear transport receptors. *Cell* **163,** 734–745 CrossRef Medline
29. Hough, L. E., Dutta, K., Sparks, S., Temel, D. B., Kamal, A., Tetenbaum-Novatt, J., Rout, M. P., and Cowburn, D. (2015) The molecular mechanism of nuclear transport revealed by atomic-scale measurements. *Elife* **4,** e10027 Medline
30. Conicella, A. E., Zerze, G. H., Mittal, J., and Fawzi, N. L. (2016) ALS mutations disrupt phase separation mediated by α-helical structure in the TDP-43 low-complexity C-terminal domain. *Structure* **24,** 1537–1549 CrossRef Medline
31. Li, H. R., Chen, T. C., Hsiao, C. L., Shi, L., Chou, C. Y., and Huang, J. R. (2018) The physical forces mediating self-association and phase-separation in the C-terminal domain of TDP-43. *Biochim. Biophys. Acta* **1866,** 214–223 CrossRef Medline
32. Schmidt, H. B., and Rohatgi, R. (2016) *In vivo* formation of vacuolated multi-phase compartments lacking membranes. *Cell Rep.* **16,** 1228–1236 CrossRef Medline
33. Lim, L., Wei, Y., Lu, Y., and Song, J. (2016) ALS-causing mutations significantly perturb the self-assembly and interaction with nucleic acid of the intrinsically disordered prion-like domain of TDP-43. *PLos Biol.* **14,** e1002338 CrossRef Medline
34. Buratti, E., and Baralle, F. E. (2012) TDP-43: gumming up neurons through protein-protein and protein-RNA interactions. *Trends Biochem. Sci.* **37,** 237–247 CrossRef Medline
35. Neumann, M., Sampathu, D. M., Kwong, L. K., Truax, A. C., Micsenyi, M. C., Chou, T. T., Bruce, J., Schuck, T., Grossman, M., Clark, C. M., McCluskey, L. F., Miller, B. L., Masliah, E., Mackenzie, I. R., Feldman, H., *et al.* (2006) Ubiquitinated TDP-43 in frontotemporal lobar degeneration and amyotrophic lateral sclerosis. *Science* **314,** 130–133 CrossRef Medline

36. Taylor, J. P., Brown, R. H., Jr, and Cleveland, D. W. (2016) Decoding ALS: from genes to mechanism. *Nature* **539,** 197–206 CrossRef Medline
37. Gopal, P. P., Nirschl, J. J., Klinman, E., and Holzbaur, E. L. (2017) Amyotrophic lateral sclerosis-linked mutations increase the viscosity of liquid-like TDP-43 RNP granules in neurons. *Proc. Natl. Acad. Sci. U.S.A.* **114,** E2466–E2475 CrossRef Medline
38. Klein-Seetharaman, J., Oikawa, M., Grimshaw, S. B., Wirmer, J., Duchardt, E., Ueda, T., Imoto, T., Smith, L. J., Dobson, C. M., and Schwalbe, H. (2002) Long-range interactions within a nonnative protein. *Science* **295,** 1719–1722 CrossRef Medline
39. Janin, J. (1979) Surface and inside volumes in globular proteins. *Nature* **277,** 491–492 CrossRef Medline
40. Wolfenden, R., Andersson, L., Cullis, P. M., and Southgate, C. C. (1981) Affinities of amino acid side chains for solvent water. *Biochemistry* **20,** 849–855 CrossRef Medline
41. Kyte, J., and Doolittle, R. F. (1982) A simple method for displaying the hydropathic character of a protein. *J. Mol. Biol.* **157,** 105–132 CrossRef Medline
42. Levitt, M. (1978) Conformational preferences of amino acids in globular proteins. *Biochemistry* **17,** 4277–4285 CrossRef Medline
43. D'Ambrogio, A., Buratti, E., Stuani, C., Guarnaccia, C., Romano, M., Ayala, Y. M., and Baralle, F. E. (2009) Functional mapping of the interaction between TDP-43 and hnRNP A2 *in vivo*. *Nucleic Acids Res.* **37,** 4116–4126 CrossRef Medline
44. Budini, M., Buratti, E., Stuani, C., Guarnaccia, C., Romano, V., De Conti, L., and Baralle, F. E. (2012) Cellular model of TAR DNA-binding protein 43 (TDP-43) aggregation based on its C-terminal Gln/Asn-rich region. *J. Biol. Chem.* **287,** 7512–7525 CrossRef Medline
45. Appocher, C., Mohagheghi, F., Cappelli, S., Stuani, C., Romano, M., Feiguin, F., and Buratti, E. (2017) Major hnRNP proteins act as general TDP-43 functional modifiers both in *Drosophila* and human neuronal cells. *Nucleic Acids Res.* **45,** 8026–8045 CrossRef Medline
46. Polling, S., Ormsby, A. R., Wood, R. J., Lee, K., Shoubridge, C., Hughes, J. N., Thomas, P. Q., Griffin, M. D., Hill, A. F., Bowden, Q., Bocking, T., and Hatters, D. M. (2015) Polyalanine expansions drive a shift into α-helical clusters without amyloid-fibril formation. *Nat. Struct. Mol. Biol.* **22,** 1008–1015 CrossRef Medline
47. He, R. Y., Huang, Y. C., Chiang, C. W., Tsai, Y. J., Ye, T. J., Gao, H. D., Wu, C. Y., Lee, H. M., and Huang, J. J. (2015) Characterization and real-time imaging of the FTLD-related protein aggregation induced by amyloidogenic peptides. *Chem. Commun.* **51,** 8652–8655 CrossRef
48. Mompeán, M., Hervas, R., Xu, Y., Tran, T. H., Guarnaccia, C., Buratti, E., Baralle, F., Tong, L., Carrión-Vazquez, M., McDermott, A. E., and Laurents, D. V. (2015) Structural evidence of amyloid fibril formation in the putative aggregation domain of TDP-43. *J. Phys. Chem. Lett* **6,** 2608–2615 CrossRef Medline
49. Mompeán, M., Buratti, E., Guarnaccia, C., Brito, R. M., Chakrabartty, A., Baralle, F. E., and Laurents, D. V. (2014) "Structural characterization of the minimal segment of TDP-43 competent for aggregation." *Arch. Biochem. Biophys.* **545,** 53–62 CrossRef Medline
50. Riback, J. A., Katanski, C. D., Kear-Scott, J. L., Pilipenko, E. V., Rojek, A. E., Sosnick, T. R., and Drummond, D. A. (2017) Stress-triggered phase separation is an adaptive, evolutionarily tuned response. *Cell* **168,** 1028–1040.e1019 CrossRef Medline
51. Neumann, M., Kwong, L. K., Lee, E. B., Kremmer, E., Flatley, A., Xu, Y., Forman, M. S., Troost, D., Kretzschmar, H. A., Trojanowski, J. Q., and Lee, V. M. (2009) Phosphorylation of S409/410 of TDP-43 is a consistent feature in all sporadic and familial forms of TDP-43 proteinopathies. *Acta Neuropathol.* **117,** 137–149 CrossRef Medline
52. Choksi, D. K., Roy, B., Chatterjee, S., Yusuff, T., Bakhoum, M. F., Sengupta, U., Ambegaokar, S., Kayed, R., and Jackson, G. R. (2014) TDP-43 Phosphorylation by casein kinase Iepsilon promotes oligomerization and enhances toxicity *in vivo*. *Hum. Mol. Genet.* **23,** 1025–1035 CrossRef Medline
53. Chen, T. C., Hsiao, C. L., Huang, S. J., and Huang, J. R. (2016) The nearest-neighbor effect on random-coil NMR chemical shifts demonstrated using a low-complexity amino-acid sequence. *Protein Pept. Lett.* **23,** 967–975 CrossRef Medline
54. Wilkins, M. R., Gasteiger, E., Bairoch, A., Sanchez, J. C., Williams, K. L., Appel, R. D., and Hochstrasser, D. F. (1999) Protein identification and analysis tools in the ExPASy server. *Methods Mol. Biol.* **112,** 531–552 Medline
55. Piotto, M., Saudek, V., and Sklenár, V. (1992) Gradient-tailored excitation for single-quantum NMR spectroscopy of aqueous solutions. *J. Biomol. NMR* **2,** 661–665 CrossRef Medline
56. Bodenhausen, G., and Ruben, D. J. (1980) Natural abundance N-15 NMR by enhanced heteronuclear spectroscopy. *Chem. Phys. Lett.* **69,** 185–189 CrossRef
57. Liu, M., Mao, X-a., Ye, C., Huang, H., Nicholson, J. K., and Lindon, J. C. (1998) Improved WATERGATE pulse sequences for solvent suppression in NMR spectroscopy. *J. Magn. Reson.* **132,** 125–129 CrossRef
58. Hyberts, S. G., Milbradt, A. G., Wagner, A. B., Arthanari, H., and Wagner, G. (2012) Application of iterative soft thresholding for fast reconstruction of NMR data non-uniformly sampled with multidimensional Poisson Gap scheduling. *J. Biomol. NMR* **52,** 315–327 CrossRef Medline
59. Hyberts, S. G., Frueh, D. P., Arthanari, H., and Wagner, G. (2009) FM reconstruction of non-uniformly sampled protein NMR data at higher dimensions and optimization by distillation. *J. Biomol. NMR* **45,** 283–294 CrossRef Medline
60. Delaglio, F., Grzesiek, S., Vuister, G. W., Zhu, G., Pfeifer, J., and Bax, A. (1995) NMRPipe: a multidimensional spectral processing system based on UNIX pipes. *J. Biomol. NMR* **6,** 277–293 Medline
61. Kjaergaard, M., Brander, S., and Poulsen, F. M. (2011) Random coil chemical shift for intrinsically disordered proteins: effects of temperature and pH. *J. Biomol. NMR* **49,** 139–149 CrossRef Medline
62. Radivojac, P., Obradovic, Z., Brown, C. J., and Dunker, A. K. (2003) Prediction of boundaries between intrinsically ordered and disordered protein regions. *Pac Symp. Biocomput.* **2003,** 216–227 Medline
63. Obradovic, Z., Peng, K., Vucetic, S., Radivojac, P., and Dunker, A. K. (2005) Exploiting heterogeneous sequence properties improves prediction of protein disorder. *Proteins* **61,** 176–182 CrossRef Medline
64. Dosztányi, Z., Csizmok, V., Tompa, P., and Simon, I. (2005) IUPred: web server for the prediction of intrinsically unstructured regions of proteins based on estimated energy content. *Bioinformatics* **21,** 3433–3434 CrossRef Medline
65. Wootton, J. C. (1994) Non-globular domains in protein sequences: automated segmentation using complexity measures. *Comput. Chem.* **18,** 269–285 CrossRef Medline

TAR DNA-binding protein 43 (TDP-43) liquid–liquid phase separation is mediated by just a few aromatic residues

Hao-Ru Li, Wan-Chin Chiang, Po-Chun Chou, Won-Jing Wang and Jie-rong Huang

J. Biol. Chem. 2018, 293:6090-6098.
doi: 10.1074/jbc.AC117.001037 originally published online March 6, 2018

Supporting Information

TAR DNA-binding protein 43 (TDP-43) liquid–liquid phase separation is mediated by just a few aromatic residues

Hao-Ru Li[1], Wan-Chin Chiang[1], Po-Chun Chou[1], Won-Jing Wang[1], and Jie-rong Huang[1,2]

From the [1]Institute of Biochemistry and Molecular Biology, National Yang-Ming University, No. 155 Section 2, Li-nong Street, Taipei, Taiwan

[2]Institute of Biomedical Informatics, National Yang-Ming University, No. 155 Section 2, Li-nong Street, Taipei, Taiwan

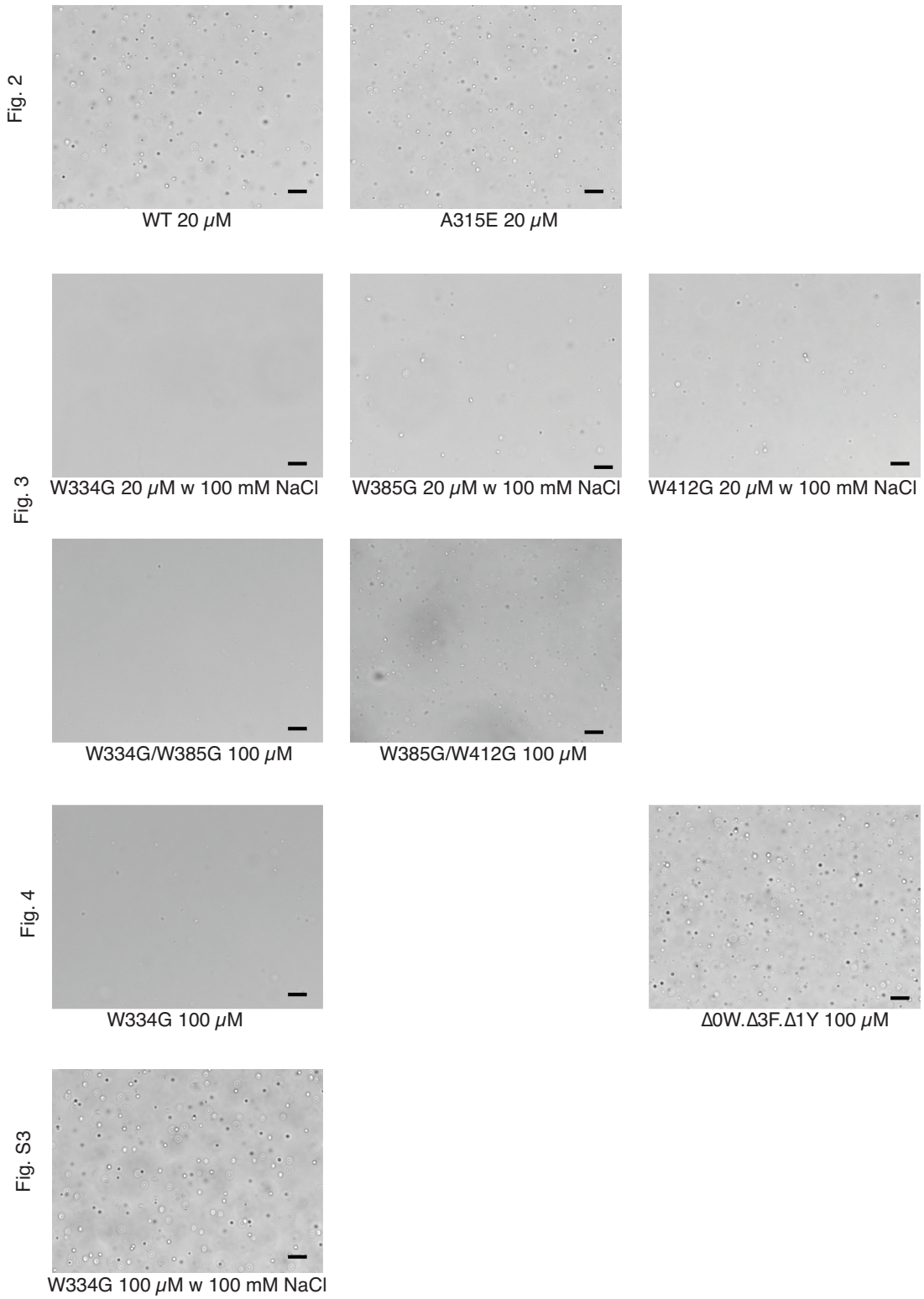

Figure S1. Uncropped micrographs used in the main text (Figs. 2–4). Scale bar: 10 μm.

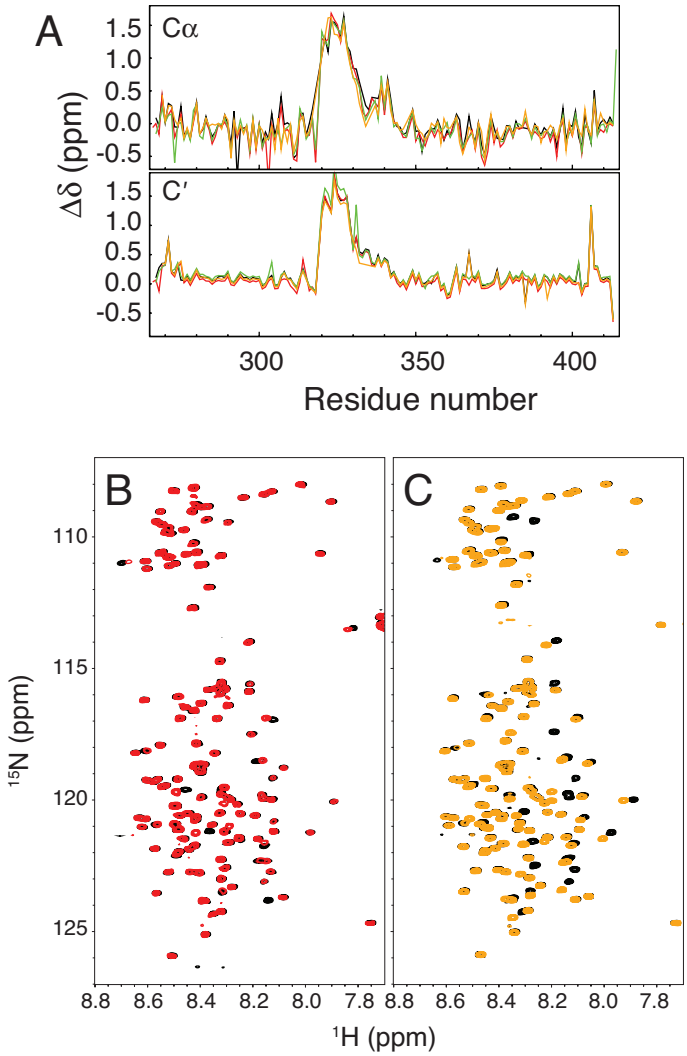

Figure S2. (A) NMR secondary chemical shifts of Cα and C' atoms for wild-type TDP-43 (black), and A315E (red), Q331K (green), and W334G (orange) variants. The data for the wild-type, Q331K, and W334G were taken from reference (1) and are shown for the sake of comparison. The overlaid ^{15}N-HSQC spectra between the wild-type (black) and (B) A315E (red) or (C) W334G (orange).

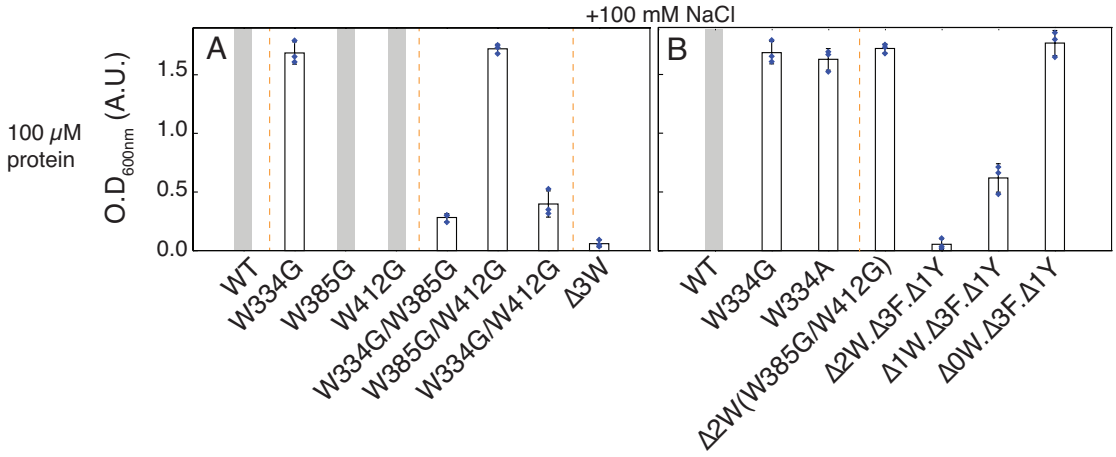

Figure S3. Sample turbidity in the presence of 100 mM NaCl. The gray bars indicate samples that precipitated before measurements could be taken.

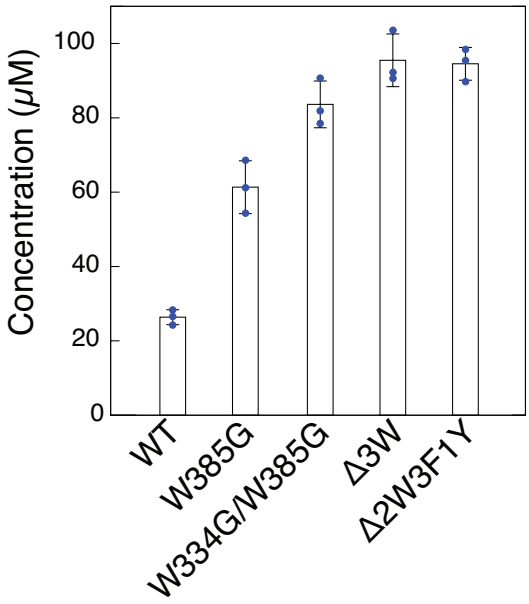

Figure S4. Centrifugation studies. Representative protein variants with concentration of 100 μM were prepared at 5 °C and centrifuged at 15000 g for 5 min. The protein concentration in the supernatant was measured. The stronger the protein's tendency to undergo LLPS is, the less protein is detected in this type of experiment.

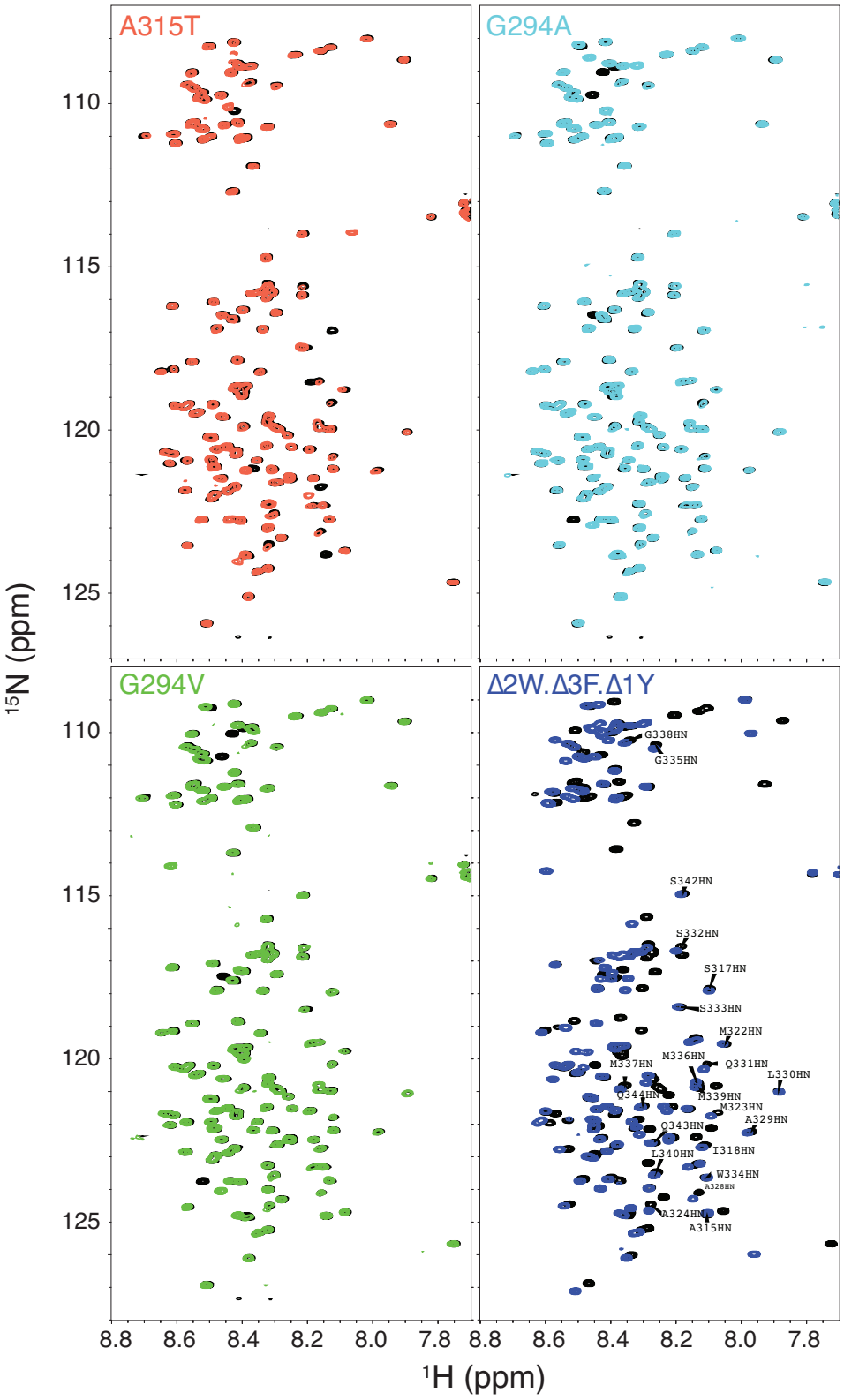

Figure S5. The comparison of HSQC spectra between A315T, G294A, G294V, Δ2W.Δ3F.Δ1Y, and the wild type. Most of the cross peaks are overlapped except those close to the mutations sites. The cross-peaks belonging to the α-helical region are indicated for the Δ2W.Δ3F.Δ1Y variant.

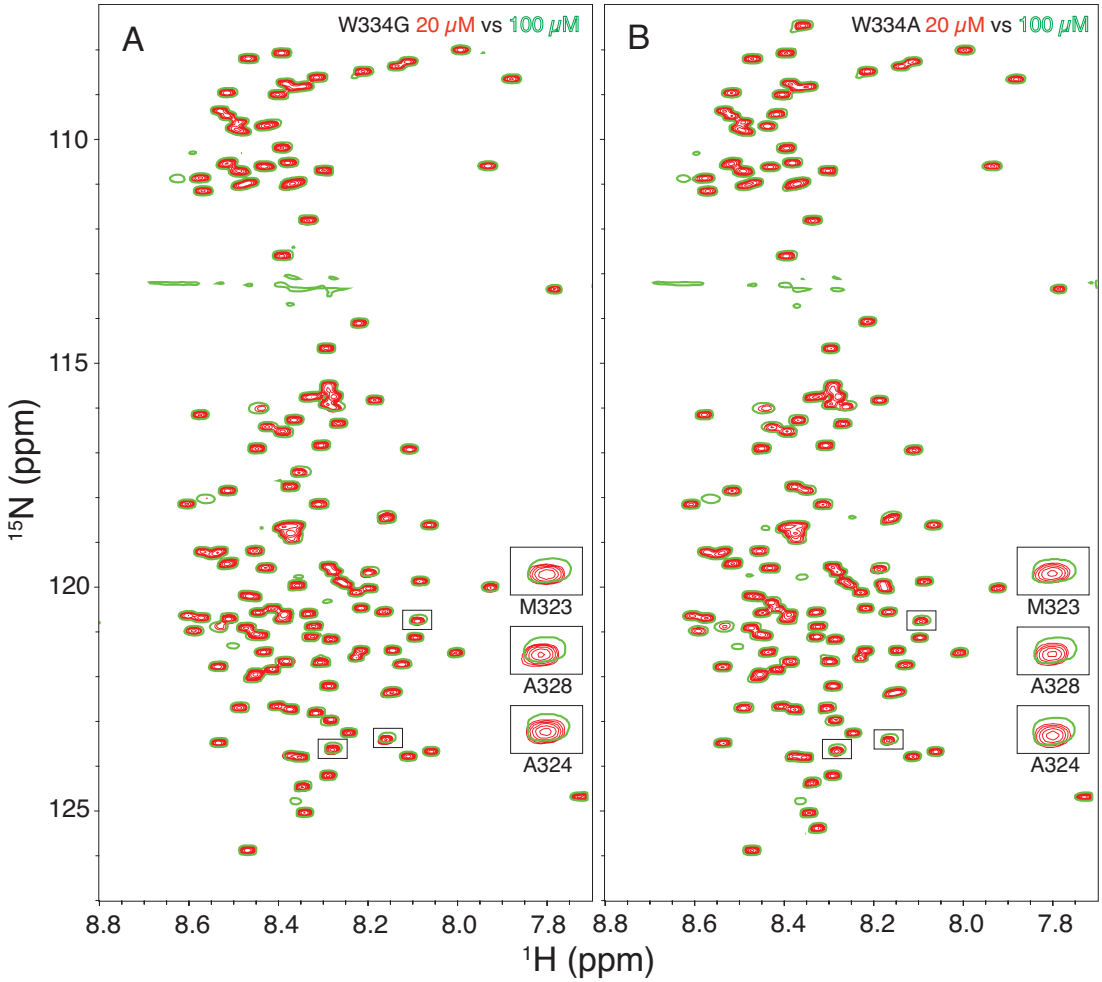

Figure S6. ^{15}N-HSQC spectra of Trp-334-replaced mutants. The spectrum recorded for the 100 μM sample is overlaid in green on those from 20 μM samples (red). The peaks (A324, A328, M323) for which the changes in chemical shifts at 288 K are the most noticeable (shown in Fig. 5*B*) are highlighted.

Table S1. The designed primers.

W334G	Fw: GCA CTA CAG AGC AGT GGC GGT ATG ATG GGC
	Rv: GCC CAT CAT ACC GCC ACT GCT CTG TAG TGC
W385G	Fw: GTG CAG CAA TTG GTG GCG GAT CAG CATC
	Rv: GAT GCT GAT CCG CCA CCA ATT GCT GCA C
W412G	Fw: GGA TTC TAA GTC TTC TGG CGG CGG AAT G
	Rv: CAT TCC GCC GCC AGA AGA CTT AGA ATC C
G385W	Fw: CAG CAA TTG GTT GGG GAT CAG CAT CC
	Rv: GGA TGC TGA TCC CCA ACC AAT TGC TG
G412W	Fw: CTT CTG GCT GGG GAA TGT AAT GAC TCG
	Rv: CGA GTC ATT ACA TTC CCC AGC CAG AAG
W334A	Fw: GCA CTA CAG AGC AGT GCG GGT ATG ATG GGC
	Rv: GCC CAT CAT ACC CGC ACT GCT CTG TAG TGC

1. Li, H. R., Chen, T. C., Hsiao, C. L., Shi, L., Chou, C. Y., and Huang, J. R. (2018) The physical forces mediating self-association and phase-separation in the C-terminal domain of TDP-43. *Biochim Biophys Acta* **1866**, 214-223